Indexed

7

DEPTH-AVERAGED MODEL FOR RIVER FLOW COMPUTATIONS (THE SHAFLOW MODEL) MODEL DEVELOPMENT AND VERIFICATIONS

by

S. B. Weerakoon

Abstract

A depth-averaged elliptic computational model in curvilinear coordinates, named the SHAFLOW model, is developed for the computation of velocity and depth computation in shallow water rivers. The grid generation module is based on a quasiconformal mapping method where the numerical solution of two partial differential equations is found to generate the boundary fitted curvilinear grids at required grid spacing. The flow computation module is based on steady flow shallow water equations written in curvilinear coordinates. An iterative algorithm similar to the SIMPLE algorithm is employed to solve these equations. This SHAFLOW model is validated by comparing the model predictions with the measurements from test problems of a gradually varying flow, two channel junction flows with flow recirculation and with irregular bed topography. It is concluded that this model with the proper parameters to represent the friction and mixing, can be used to obtain sufficiently accurate information of velocity and water surface elevation in two dimensions for design purposes applied to shallow water rivers. A case study application of the model is summarized in an accompanying paper in the same issue.

Notation

D Grid aspect ratio

d_η, d_ξ coefficients derived from momentum equations for depth-averaged pressure correction equation

g gravitational acceleration

$g_{\xi\xi}, g_{\eta\eta}$ metric coefficients in transformation

H water depth

H^* H guessed or at current iteration level

$H/$ correction for H at current iteration level

n Manning's roughness coefficient

R_ξ, R_η radii of curvature in η, ξ coordinate lines

u, v depth-averaged velocity components in η, ξ, directions

U^* shear velocity

u^*, v^* u, v guessed or at current iteration level

$u/, v/$ correction for u, v at current iteration level

$S\psi$ mass residual

α underrelaxation factor

β non-dimensionalized effective viscosity

ε effective viscosity

ξ, η curvilinear coordinates

ζ water surface elevation

Manuscript received : 08.08.2002
Manuscript accepted : 05.02.2003

1. Introduction

A detailed understanding of the flow pattern and water depths at different discharges in river reaches is necessary for hydraulic engineers in the design of appropriate flood control measures, estimation of erosion and sedimentation, identifying favourable regions for different aquatic habitats, etc.. This is accomplished either by physical (scale) modelling or by computational modeling. With the advances in computers and numerical solution methods, the latter has become more economical and widely used today, though it is not a complete replacement of the former in hydraulic engineering.

Computational models for rivers are essentially based on the theoretical formulations relating to the flow, fluid and geometric parameters derived by the application of conservation laws and some constitutive relationships. Such models of varying complexities have been applied to predict river flows over the last few

Eng. (Dr.) S. B. Weerakoon, BSc (Eng.), MEng., PhD (Tokyo), CEng., MSLAAS, MIESL, Presently Senior Lecturer in Civil Engineering, University of Peradeniya.

decades. Natural river flows are complex and three dimensional, for example velocity varies across it, from the bottom to the free surface and along the river. Thus it is the usual practice that varying approximations, justifiable to the river flow situation in hand, are made to the equations in order to obtain the solution conveniently at reasonable accuracy. Among the computational models available, one-dimensional river models based on the Saint Venant equations have been applied to river systems for gross prediction of flood water levels, discharge distributions and sediment transport along rivers (Cunge et al., 1980). The applications of three-dimensional computational studies have, mostly, been limited to laboratory channel flows with rectangular cross-sections. This is mainly due to the numerical instabilities encountered in the computations when the irregular bed topography inherent to natural rivers is taken into account. On the other hand, the depth-averaged models, which are economical, also provide sufficient details of flow velocities and flows in shallow water rivers, efficiently and to a reasonable accuracy. Many recent applications of depth-averaged models to laboratory channel flows can be found in the papers by Molls and Chaudhry (1995), Zhou (1995), Babarutsi et al. (1996), Ye and McCorquodale (1997), and Lien et al. (1999). The application of depth averaged models in Cartesian coordinates to natural rivers have been presented by Vreugdenhil and Wijbenga (1982), ASCE(1989). Also, Wijbenga (1985) and Wenka et al. (1993) presented applications in curvilinear coordinates which are more suitable in applications to rivers. Nevertheless, the detailed description of computational procedures is not given in them, and also, no description on curvilinear grid generation is given as they have used commercial grid generation packages. In contrast, this Paper presents, in detail, a boundary-fitted closely orthogonal grid generation procedure, the development of a depth-averaged model and a solution procedure similar to the SIMPLE (Semi-implicit method for pressure-linked equations, Patankar 1980) for flow computation in natural river reaches. Finally the model's capability has been demonstrated by its applications to several flow situations where comparison with measurement was possible. They include a gradually varying flow in a straight channel, flow in a channel junction with a flow recirculation zone and a flow in a channel junction with an irregular bed including a scour hole resembling a bed topography of a natural river confluence.

2. Governing Equations

The three momentum equations and the continuity equation written for general three-dimensional flow are integrated over time and depth to derive the depth-averaged equations commonly known as the steady flow shallow water equations applicable to shallow free surface flows (Vreugdenhil, 1994). In the derivation, the vertical acceleration of water is assumed to be negligible compared with the gravitational acceleration and that yields the hydrostatic pressure distribution. The effective stress tensor components in depth averaged equations are modelled by a gradient-diffusion model (Kuiper and Vreugdenhil 1973, Molls and Chaudhry 1995). The shear stress on the free surface is neglected and the bottom shear stress is modelled by relating it to the local free surface slope. Then, the local free surface slope is computed from Manning's formula. The shallow water equations in orthogonal curvilinear coordinates for steady state flow are given in Eqns. (1) to (3). The details of derivation of shallow water equations can be found in Kuiper and Vreugdenhil (1973), Vreugdenhil (1994) and Cunge et al. (1980). Similar equations can also be found in Vreugdenhil and Wijbenga (1982), and Wijbenga (1986). These are, using notation given at the beginning

$$\frac{1}{\sqrt{g_{\bullet}}}\frac{\partial}{\partial \xi}\left\{Hu\sqrt{g_{\eta\eta}}\right\}+\frac{1}{\sqrt{g_{\bullet}}}\frac{\partial}{\partial \eta}\left\{Hv\sqrt{g_{\xi\xi}}\right\}=0 \qquad (1)$$

$$\frac{u}{\sqrt{g_{\xi\xi}}}\frac{\partial u}{\partial \xi}+\frac{v}{\sqrt{g_{\eta\eta}}}\frac{\partial u}{\partial \eta}+\frac{uv}{R_{\xi}}-\frac{v^{2}}{R_{\eta}}+Cu+\frac{g}{\sqrt{g_{\xi\xi}}}\frac{\partial \varsigma}{\partial \xi}=\frac{\varepsilon}{\sqrt{g_{\xi\xi}}}\frac{\partial}{\partial \xi}A-\frac{\varepsilon}{\sqrt{g_{\eta\eta}}}\frac{\partial}{\partial \eta}F \qquad (2)$$

$$\frac{u}{\sqrt{g_{\xi\xi}}}\frac{\partial v}{\partial \xi}+\frac{v}{\sqrt{g_{\eta\eta}}}\frac{\partial v}{\partial \eta}+\frac{uv}{R_{\eta}}-\frac{u^{2}}{R_{\xi}}+Cv+\frac{g}{\sqrt{g_{\eta\eta}}}\frac{\partial \varsigma}{\partial \eta}=\frac{\varepsilon}{\sqrt{g_{\eta\eta}}}\frac{\partial}{\partial \eta}A+\frac{\varepsilon}{\sqrt{g_{\xi\xi}}}\frac{\partial}{\partial \xi}F \qquad (3)$$

where

$$C = \frac{gn^2}{H^{4/3}}\sqrt{u^2+v^2}$$

$$\frac{1}{R_\xi} = \frac{1}{\sqrt{g\cdot}}\frac{\partial\sqrt{g_{\xi\xi}}}{\partial\eta}$$

$$\frac{1}{R_\eta} = \frac{1}{\sqrt{g\cdot}}\frac{\partial\sqrt{g_{\eta\eta}}}{\partial\xi}$$

$$A = \frac{1}{\sqrt{g\cdot}}\left\{\frac{\partial}{\partial\xi}\left(u\sqrt{g_{\eta\eta}}\right)+\frac{\partial}{\partial\eta}\left(v\sqrt{g_{\xi\xi}}\right)\right\}$$

$$F = \frac{1}{\sqrt{g\cdot}}\left\{\frac{\partial}{\partial\xi}\left(v\sqrt{g_{\eta\eta}}\right)-\frac{\partial}{\partial\eta}\left(u\sqrt{g_{\xi\xi}}\right)\right\}$$

$$g\cdot = g_{\xi\xi}\cdot g_{\eta\eta}$$

3. Grid generation and coordinate transformation for flow computation

Numerical grid generation and coordinate transformation are useful for creating a boundary-fitted curvilinear coordinate system and obtaining the numerical solution of the partial differential equations governing the flow at arbitrary-shaped regions in computational fluid dynamics. The main advantage in using such a coordinate system compared with the Cartesian coordinate system is that numerical algorithms can be applied to general configurations without the need of special procedures at the boundaries. For, accurate numerical computations, the grid lines in the physical domain are placed at closer intervals in the regions of high gradients than in other regions. However, these curvilinear grid lines are transformed to straight grid lines at unit spacing in the computational domain for the coding of the algorithm to be simple.

Grid generation in closed boundary problems is accomplished by the solution of elliptic partial differential equations (Thompson et al., 1982). We use here a quasiconformal mapping method where the grid spacing at the boundaries can be easily controlled to obtain the required grid spacing though the grid lines will slightly deviate from the orthogonality requirement.

Consider the metric relations referred to the curvilinear coordinate system (ξ, η) and Cartesian coordinate system (x,y) in Fig.1. For an orthogonal curvilinear coordinate system, we can write the Eqns. (4) to (6) given below using the base vectors

$$\mathbf{g}_\xi = \frac{\partial x}{\partial\xi}\mathbf{i}_x + \frac{\partial y}{\partial\xi}\mathbf{i}_y,\ \mathbf{g}_\eta = \frac{\partial x}{\partial\eta}\mathbf{i}_x + \frac{\partial y}{\partial\eta}\mathbf{i}_y:$$

where, $g_{\xi\xi}=g_\xi \cdot g_\xi$ and $g_{\eta\eta}=g_\eta \cdot g_\eta$ are metric tensor components. Interested readers may refer to Sokolonikoff (1964) for more on coordinate transformations.

Defining grid aspect ratio, $D=\sqrt{g_{\xi\xi}/g_{\eta\eta}}$, the following two elliptic partial differential equations can be obtained from Eqns. (4) to (6).

$$\left(\frac{\partial x}{\partial\xi}\right)^2+\left(\frac{\partial y}{\partial\xi}\right)^2 = g_{\xi\xi} \tag{4}$$

$$\left(\frac{\partial x}{\partial\eta}\right)^2+\left(\frac{\partial y}{\partial\eta}\right)^2 = g_{\eta\eta} \tag{5}$$

$$\frac{\partial x}{\partial\xi}\cdot\frac{\partial x}{\partial\eta}+\frac{\partial y}{\partial\xi}\cdot\frac{\partial y}{\partial\eta} = 0 \tag{6}$$

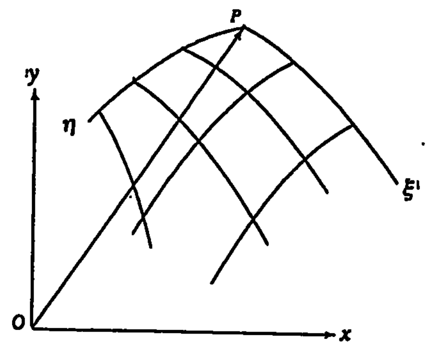

(a) Cartesian coordinates y^i and curvilinear coordinates

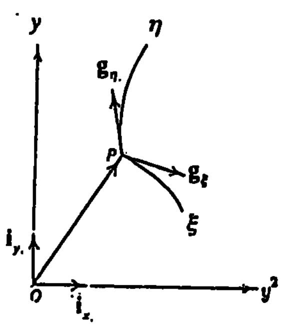

(b) Base vectors.

Figure 1. Coordinate transformation

$$\frac{\partial}{\partial\xi}\left(\frac{1}{D}\frac{\partial x}{\partial\xi}\right)+\frac{\partial}{\partial\eta}\left(D\frac{\partial x}{\partial\eta}\right)=0 \tag{7}$$

$$\frac{\partial}{\partial\xi}\left(\frac{1}{D}\frac{\partial y}{\partial\xi}\right)+\frac{\partial}{\partial\eta}\left(D\frac{\partial y}{\partial\eta}\right)=0 \tag{8}$$

Eqns (7) and (8) form a Beltrami system of equations describing a quasiconformal mapping between two coordinate systems (Note that D=1 corresponds to conformal mapping). D is a measure of the nonsmoothness of a grid system and a monotonous variation of D over the domain guarantees smooth grids. The partial differential equations (7) to (8) are descretized employing the central-difference scheme on the finite difference mesh shown in Fig.2 to yield algebraic equations for the coordinates x and y connecting each coordinate with four surrounding coordinates.

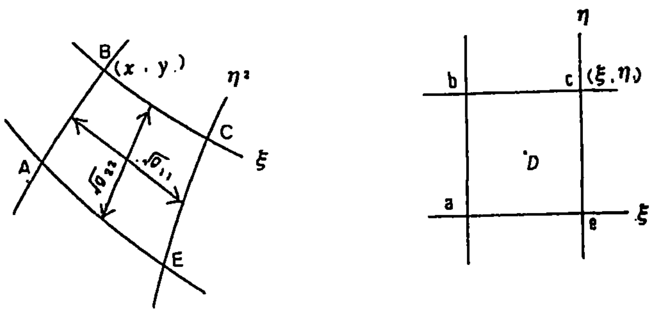

a) Physical plane

b) Transformed plane

Figure 2. Finite-difference grid;.

Solution procedure

The numerical solution of the algebraic equations is found for generating the curvilinear grid in the given flow region as follows.

Step 1: Specify the coordinates of the boundary points of the grid lines to be generated. Note that this controls the spacing between grids. Create a rough grid by interpolation.

Step 2: Compute the grid aspect ratio *(D)* for each grid and create a monotonous variation of *D* in the domain. For example, apply a five point smoother for *D*.

Step 3: Solve the algebraic equations of 7 and 8 for x and y. For example, apply double sweeps of the Tridiagonal Matrix Algorithm *(TDMA)* solver which is based on Gaussian elimination (Versteeg and Malalasekera, 1995).

Step 4: Decide the suitability of the grid based on the grid spacing and orthogonality of the internal grids by direct observation, or alternatively, by computing orthogonality index .

Step 5: Repeat from Step 3 (that is iterate) until satisfactory grid is obtained. A few iterations (3 or 4) are usually sufficient.

Step 6: Compute metric coefficients of transformation required for the governing equations. Save the coordinates and coefficients of the generated grid.

Fig.3 shows a 33x65 grid generated at a confluence region (the Tone and Watarase river confluence in Japan) by the above method after three iterations. The grid lines have been closely spaced in the mixing region of tributary flows and wall regions where the gradients of flow velocities are high. The grid also possesses sufficient orthogonality for use in flow computation using Eqns. (1) to (3).

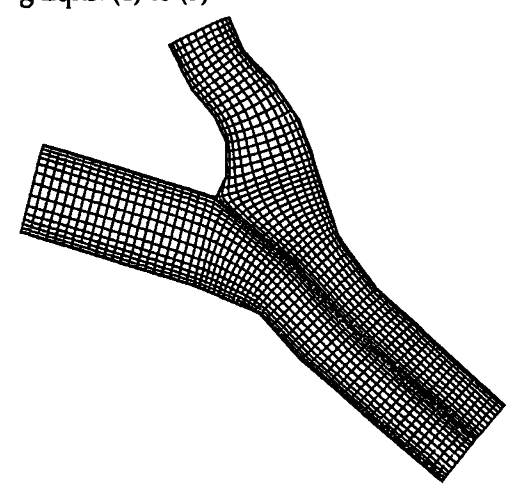

Figure 3. An example of a generated grid (The Tone and Watarase river confluence)

4. Flow computation

Discretization of Equations

The shallow water equations given in Eqns. (1) to (3) are solved in the transformed domain for obtaining the distribution of velocity components and the flow depth. The equations are descretized on the uniform staggered grids shown in Fig.4. The momentum equations are descretized using the upwind difference scheme for convection terms and the central-difference scheme for diffusion terms. The continuity equation is descretized using the central difference scheme. More details on numerical schemes and descretization on a staggered grid can be found in Patankar (1980), Roache (1972) and Versteeg and Malalasekera (1995).

The continuity equation becomes

$$H_e u_P \sqrt{g_{\eta\eta_e}} - H_e u_W \sqrt{g_{\eta\eta_w}} + H_n v_P \sqrt{g_{\xi\xi_n}} - H_s v_S \sqrt{g_{\xi\xi_s}} = 0 \qquad (9)$$

where

$$H_e = \left(H_p + H_E\right),\ H_w = \left(H_p + H_W\right),\ H_n = \left(H_p + H_N\right),\ H_s = \left(H_p + H_S\right)$$

and H is the water depth and u and v are velocity components in the ξ and η directions.

The subscript denotes the location of the variables.

The ξ-direction momentum equation becomes

$$a_P u_P = a_E u_E + a_W u_W + a_N u_N + a_S u_S + S_{\phi u} \tag{10}$$

where,

$$a_E = \max(0, -u_p/\sqrt{g_{\xi\xi_e}}), \qquad a_W = \max(0, u_p/\sqrt{g_{\xi\xi_e}})$$

$$a_N = \max(0, -\bar{v}/\sqrt{g_{\eta\eta_e}}), \qquad a_S = \max(0, \bar{v}/\sqrt{g_{\eta\eta_e}})$$

$$a_P = a_E + a_W + a_N + a_S + \frac{gn^2\sqrt{u_P{}^2 + \bar{v}^2}}{\left(0.5(H_P + H_N)\right)^{(4/3)}}$$

$$\bar{v} = (v_P + v_S + v_E + v_{SE})/4$$

$$S_{\varphi u} = \frac{g}{\sqrt{g_{\xi\xi_e}}}(\zeta_P - \zeta_E) + s_{\varphi u}$$

$s_{\varphi u}$ = other terms

The η-direction momentum equation becomes

$$b_P v_P = b_E v_E + b_W v_W + b_N v_N + b_S v_S + S_{\phi v} \tag{11}$$

where,

$$b_E = \max(0, -\bar{u}/\sqrt{g_{\xi\xi_n}}), \qquad b_W = \max(0, \bar{u}/\sqrt{g_{\xi\xi_n}})$$

$$b_N = \max(0, -v_p/\sqrt{g_{\eta\eta_n}}), \qquad b_S = \max(0, v_p/\sqrt{g_{\eta\eta_n}})$$

$$b_P = b_E + b_W + b_N + b_S + \frac{gn^2\sqrt{\bar{u}^2 + v_P{}^2}}{\left(0.5(H_P + H_N)\right)^{(4/3)}}$$

$$\bar{u} = (u_P + u_W + u_N + u_{NW})/4$$

$$S_{\varphi v} = \frac{g}{\sqrt{g_{\eta\eta_n}}}(\zeta_P - \zeta_N) + s_{\varphi v}$$

$s_{\varphi v}$ = other terms

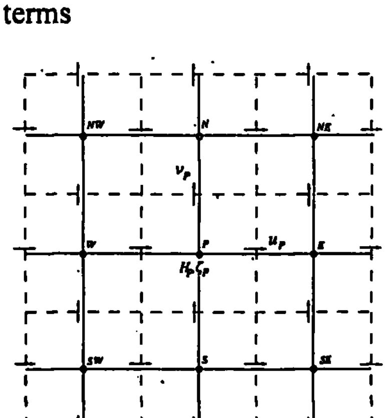

Figure 4. Definition of variables in staggered grid

Solution Algorithm

The algebraic equations given in Eqns. (10) and (11) can be solved to obtain the velocity fields u and v and if the free surface elevation or depth (ζ or H) field is given. This velocity field should satisfy the continuity equation, which is Eqn. (9). Therefore, the free surface elevation distribution is guessed and corrected by an iterative algorithm. An iterative algorithm is derived below for the depth-averaged flow computation following the same steps of the SIMPLE used for solving flow equations that are not spatially averaged.

Underrelaxation

In finding a numerical solution by an iterative process for the momentum equations which are nonlinear partial differential equations, underrelaxation of the solution at each iterative step is practised by introducing an underrelaxation factor: $\alpha\,(0<\alpha<1)$. A lucid discussion on underrelaxation can be found in Roache (1972). Thus, introducing

$$u_P = u_P^{\bullet} + \alpha_u(u_P - u_P^{\bullet})$$

$$v_P = v_P^{\bullet} + \alpha_v(v_P - v_P^{\bullet})$$

the above algebraic Eqns. (10) and (11) become,

$$\frac{a_P}{\alpha_u}u_P = a_E u_E + a_W u_W + a_N u_N + a_S u_S + S_{\phi u} + (1-\alpha_u)\frac{a_P}{\alpha_u}u_P^{\bullet} \tag{12}$$

$$\frac{b_P}{\alpha_v}v_P = b_E v_E + b_W v_W + b_N v_N + b_S v_S + S_{\phi v} + (1-\alpha_v)\frac{b_P}{\alpha_v}v_P^{\bullet} \tag{13}$$

where, α_u are α underrelaxation factors for u_p and v_p are the u_p and v_p values from the previous iteration.

Velocity - depth coupling

The velocity-depth coupling has drawn much attention in the reported depth-averaged computations employing SIMPLE-like procedures as it is the most crucial component in the algorithm with respect to the convergence of the numerical solution (ASCE 1989, Wenka et al. 1995, Zhou 1995 and Ye and McCorquodale 1997). Thus, an efficient form of the velocity coupling equation, named the depth correction equation, given in Weerakoon et al. (1991) is used.

The depth correction equation

$$\frac{\partial}{\partial\xi}\sqrt{g_{\eta\eta}}\left\{u^{\bullet}H' - (H^{\bullet}d_{\xi})\frac{\partial H'}{\partial\xi}\right\} + \frac{\partial}{\partial\eta}\sqrt{g_{\xi\xi}}\left\{v^{\bullet}H' - (H^{\bullet}d_{\eta})\frac{\partial H'}{\partial\eta}\right\}$$
$$= -\frac{\partial}{\partial\xi}\sqrt{g_{\eta\eta}}(H^{\bullet}u^{\bullet}) - \frac{\partial}{\partial\eta}\sqrt{g_{\xi\xi}}(H^{\bullet}v^{\bullet}) \tag{14}$$

The depth and velocity corrections are

$$H = H^* + H^{\prime} \tag{15}$$

$$u = u^* - d_\xi \frac{\partial H^{\prime}}{\partial \xi} \tag{16}$$

$$v = v^* - d_\eta \frac{\partial H^{\prime}}{\partial \eta} \tag{17}$$

where

$$d_\xi = \frac{\alpha_u g}{a_P \sqrt{g_{\xi\xi_e}}}$$

$$d_\eta = \frac{\alpha_v g}{b_P \sqrt{g_{\eta\eta_n}}}$$

and u^*, v^* and H^* are velocity components and the depth at the current iteration level that need to be corrected to satisfy the continuity equation. $H^{\prime}$ is the depth correction required.

The depth correction equation is descretized on the control volume shown in Fig.4 employing the Hybrid scheme (Patankar, 1980) to yield the following algebraic equation.

$$c_E = \max(abs(0, 0.5u_P^* \sqrt{g_{\eta\eta_e}}), d_{\xi_P} H_e^* \sqrt{g_{\eta\eta_e}}) - 0.5u_P^* \sqrt{g_{\eta\eta_e}}$$

$$c_W = \max(abs(0, 0.5u_W^* \sqrt{g_{\eta\eta_w}}), d_{\xi_W} H_w^* \sqrt{g_{\eta\eta_w}}) + 0.5u_W^* \sqrt{g_{\eta\eta_w}}$$

$$c_N = \max(abs(0, 0.5v_P^* \sqrt{g_{\xi\xi_n}}), d_{\xi_P} H_n^* \sqrt{g_{\xi\xi_n}}) - 0.5v_P^* \sqrt{g_{\xi\xi_n}}$$

$$c_S = \max(abs(0, 0.5v_S^* \sqrt{g_{\xi\xi_s}}), d_{\xi_S} H_s^* \sqrt{g_{\xi\xi_s}}) + 0.5v_S^* \sqrt{g_{\xi\xi_s}}$$

$$c_P = c_E + c_W + c_N + c_S + u_P^* \sqrt{g_{\eta\eta_e}} - u_W^* \sqrt{g_{\eta\eta_w}} + v_P^* \sqrt{g_{\xi\xi_n}} - v_S^* \sqrt{g_{\xi\xi_s}}$$

$$S_{\varphi c} = c_E H_e^* - c_W H_w^* + c_N H_n^* - c_S H_s^*$$

The term $S_{\varphi c^{\prime}}$, which is the right hand side of Eqn. (14), is the descretized form of the continuity equation. $S_{\varphi c^{\prime}}$, represents the residual mass and approaches zero at convergence. The total of the absolute value of residual masses in the domain is considered to serve as the indicator for the convergence of the solution.

When $H^{\prime}$ distribution is found, the velocity fields are corrected by the following descretized forms of Eqns. (16) and (17).

$$u = u^* + d_\xi \left(H_P^{\prime} - H_E^{\prime} \right) \tag{19}$$

$$v = v^* + d_\eta \left(H_P^{\prime} - H_N^{\prime} \right) \tag{20}$$

Solution Procedure

The flow computational problem is defined for the model by reading the curvilinear grid coordinates, the bed elevations and transformation coefficients created by the grid generation module, the roughness coefficient, the effective viscosity and the discharge and downstream water depth (or free surface elevation). An iterative solution of the set of algebraic equations (10), (11), (18) is found following the steps similar to the SIMPLE procedure as given below.

1. Guess the depth field H^* and velocity fields u^*, v^*
2. Solve the momentum equations
3. Solve the depth correction equation
4. Correct velocities u^*, v^* and depth H^*. For a few initial iterations the depth may be updated with a relaxation factor: $\alpha_h H = H^* + \alpha_h H^{\prime}$. Choose α_h such that $0.3 \le \alpha_h \le 0.5$.
5. Considering the corrected depth and velocity fields as new guess depth field H^* and velocity fields u^*, v^* return to step 2 and repeat until convergence is reached.

5. Boundary conditions

The boundary conditions used for solving the shallow water equations have been discussed by many researchers (Vreugdenhil and Wijbenga 1982, Molls and Chaudry 1995, Ye and McCorquodale 1997). For a subcritical flow, the boundary conditions for the present model are summarized below.

At the upstream: The unit discharge distribution, i.e., Hu and Hv, are given for momentum equations. This follows the boundary condition $(Hu)^{\prime} = 0$ for the depth correction equation.

At the downstream: For the momentum equations, the flow is assumed to be developed. That is streamwise gradients of u and v are set to zero. The water surface elevation is specified, therefore, $H^{\prime}$ downstream is zero.

At the banks: The velocity component perpendicular to the wall is set to zero. The streamwise velocity is specified by the no-slip condition with the wall function method (Launder and Spalding, 1974) for laboratory flow computations and by the free-slip condition for natural river flow computations. In the no-slip condition, the streamwise velocity at the first grid point at a distance y_p from the wall is related to the friction velocity U^* according to $u/U_* = (1/\kappa) \ln (Ey^+)$, where κ is the von Karmann constant which is 0.42, y^+ is the non-dimensional wall distance $U_* y_p / \nu$ ($30 \le y^+ \le 100$) and E is the roughness parameter which is 9 for hydraulically smooth walls. In the free-slip condition (Vreugdendhil and Wijbenga, 1982) applied to large water bodies where boundary friction has little influence on the flow, the friction is neglected at the boundary allowing flow to slip freely.

For the depth correction equation: (Hv) / = 0 at the walls.

6. Manning's coefficient and effective viscosity

Manning's friction coefficient and the effective viscosity appearing in the shallow water equations have to be specified depending on the flow. Vreugdenhil and Wijbenga (1982), considering a single river reach, investigated their sensitivity on velocity and depth and showed that when n or ε is increased the water depth increases and the velocity profile become more even. Babarutsi et al. (1996) have shown that shallow water flows are dominantly influenced more by bottom friction than by mixing. Manning's roughness coefficient n, with the absence of other information, may be selected referring to the values recommended for one-dimensional flow computations. When applied to depth-averaged flow computations, n values lower by 1-2% of those recommended for one-dimensional computations are found to produce superior results. Nevertheless, n for the given flow should be finally adjusted in the model calibration process.

The effective eddy viscosity ε is specified using the relationship, $\varepsilon/U^*H=\beta$ where H is the water depth, U^* is the shear velocity and β is a nondimensional diffusion coefficient that depends on the flow. Fischer et al. (1979) documented a table of diffusion coefficients (β) or a wide range of flows based on a large number of laboratory and field experiments.

7. Model Validation

Test I. Flow in prismatic channel

A prismatic channel of length 48 m with a rectangular cross section of width 1.5 m and slope 1/250 carrying a discharge of 21 l/s under subcritical flow controlled by a gate at the outlet is considered. The gradually varied flow was computed for three different downstream depths at the gate; H =3 cm, 6 cm and 9 cm.

The complete model consisting of the grid generation module and the flow computation modules was applied. A grid of 160x27 was generated with closely spaced grid lines near the walls. Note that first grid near each wall has to satisfy the condition $30 \leq y^+ \leq 100$ for the wall function method to be applicable as the boundary condition. The roughness coefficient, n = 0.012 and effective viscosity β = 0.1 (Fisher et al., 1979) which corresponds to ε = 1 cm²/s were used. The solution converged to provide a residual mass less than 0.01% showing the stable and efficient performance of the model. The plot of the computed depth variation along the channel is shown in Fig.5. The flow approaches a uniform depth of 2.86 cm (Fr = 0.9) upstream in each of the three cases. The one-dimensional uniform flow equation, viz. Manning's equation, for same roughness value, unit discharge and the slope gives a uniform depth of 2.85 cm and thus the agreement is satisfactory. A roughness coefficient n which is smaller than 1% from the value used for one-dimensional computations was found to give the upstream uniform depth of 2.85 cm as discussed in the previous section.

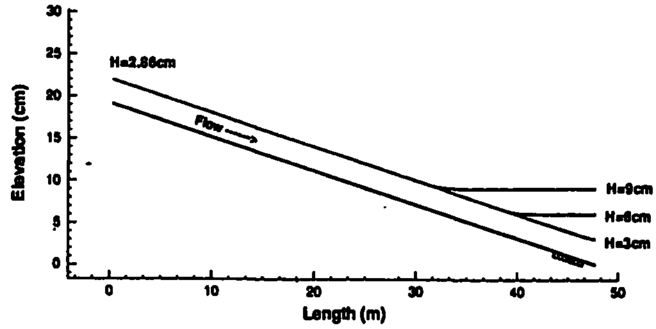

Figure 5. Free surface profiles in Test Case I

Test II. Channel junction flow with flow recirculation

The model prediction was validated against the measurements of velocity and depth of a laboratory channel junction flow (channel confluence) with rectangular cross section. The main channel is 0.5 m wide and the tributary channel is 0.3 m wide. The tributary joins the main channel at an angle of 60 deg. The lengths of the main channel to the upstream and downstream of the junction are 7 m and 8 m respectively, the length of the tributary channel is 4 m as shown in Fig.6. A steady channel flow corresponding to the conditions given in Table 1 was maintained by a recirculating pump with the valve arrangements shown. The depth-averaged velocity measurements were carried out by a two component magnetic current meter. More details of the experiment can be found in Weerakoon et al. (1990).

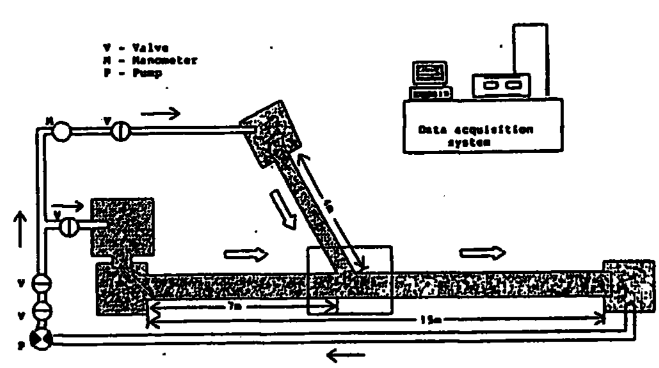

Figure 6. Channel configuration for Test Cases II and III

Table 1. Flow conditions of the Test Cases II and III

Test Case	Main channel			Branch channel		
	Discharge (l/s)	Depth (cm)	Initial bed slope	Discharge (l/s)	Depth (cm)	Initial bed slope
II	4.4	5.0 u/s, 4.6 d/s	1/1000	2.5	5.0	1/1000
III	5.5	2.8 u/s, 3.7d/s	1/200	3.3	2.9	1/200

The model was applied to compute the velocity and water depth in the junction region using a computational grid covering channel lengths of 140 cm and 220 cm from the downstream corner of the confluence to the upstream and downstream respectively. A part of computational grid of 60 x 30 is shown in Fig. 7. The upstream discharge distributions and the downstream depth were given as boundary conditions for the model. Manning's roughness coefficient, n = 0.011 and (= 0.1.

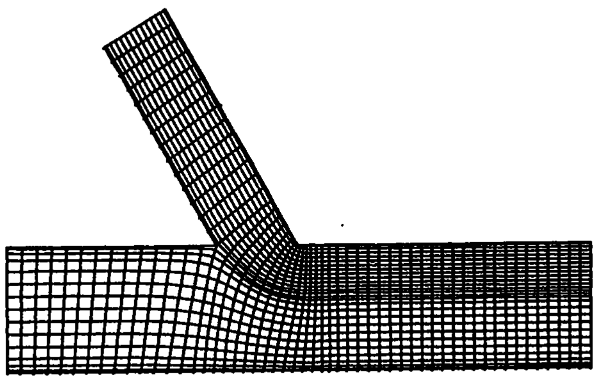

Figure 7: Part of computational grid for Test Cases II and III

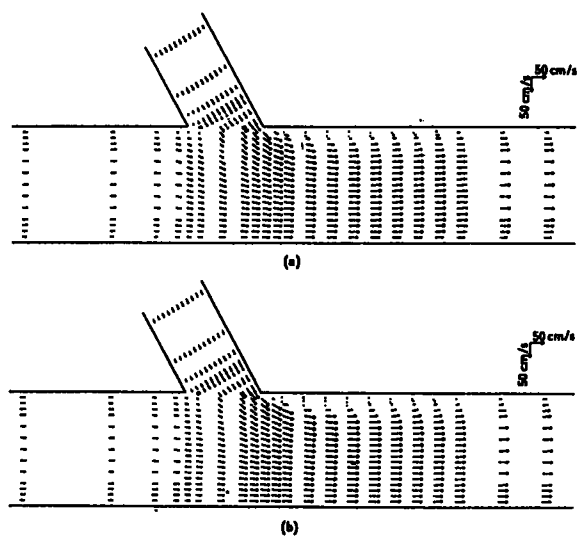

Figure 8. Velocity vectors in Test Case II; a) Computed b) Measured

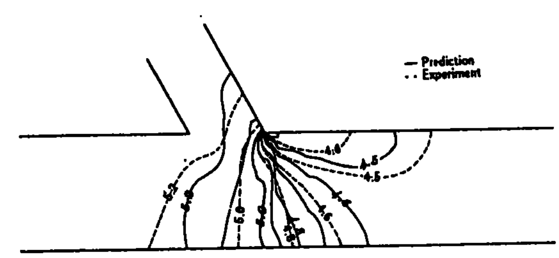

Figure 9. Free surface elevation contours of Case II. (Contours are in cm)

Comparisons of computed and measured depth-averaged velocity field and free surface elevation of Test Case II are depicted in Figs. 8 and 9. The velocities are plotted exactly at the points where discrete values are available from the experiments and the comparison shows good agreement. However, the computation has underestimated the size of the recirculation zone which is very much influenced by the diffusivity and also by the bottom roughness coefficient n by about 20% less than that of the experiment. The sensitivity of β was tested by using different values in the range given in Fisher et al. (1979). The difference between the results was the decrease in the size of the recirculation zone, for example, $\beta = 0.4$ resulted in a 10% reduction in the size of the recirculation zone. The numerical diffusion generated when the flow is inclined to grid lines is also responsible for this discrepancy. Except for an over prediction of the depth in the recirculation region, superelevations are well predicted and the free surface elevation contours closely match with the observation in general. Overall agreement of the model predictions in this complex flow is satisfactory.

Test III. Channel junction flow with an irregular bed topography

At the next step, the model was validated by its application to a complex flow condition in a channel junction with a mobile bed at dynamic equilibrium. The channel dimensions are the same as in Test II above, but the channel bed was covered with sand of 1.6mm mean diameter. The details of the flow at the dynamic equilibrium condition are given in Table 1. The bed topography of the junction shown in Fig. 10 has features in a natural river confluence (Best, 1988). The depth averaged velocity field and the depths were measured by fixing the bed as described in Weerakoon et al. (1990).

Table 2. Specification of Manning coefficient and eddy viscosity

Test case	n (SI units)	ε cm^2/s	$\beta = \varepsilon / U_* H$
II	0.011	1	0.1
III-1	0.013 u/s, 0.016d/s	3 u/s, 8d/s	0.2 u/s, 0.5 d/s
III-2	0.013 u/s, 0.016d/s	3	0.2
III-3	0.013 u/s, 0.016d/s	8	0.5
d/s = at downstream, u/s = at upstream, r/c= river channel, f/p flood plain			

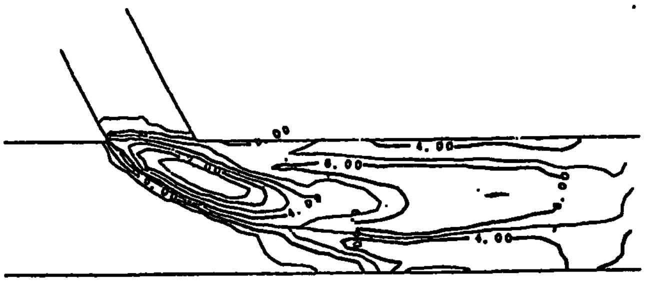

Figure 10.. Bed topography of the channel in Test Case III

(Contours are in cm)

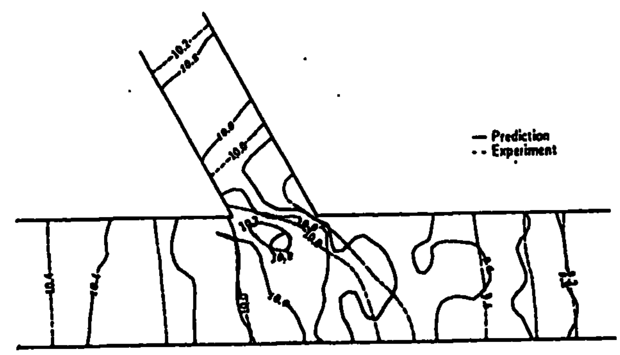

Figure 12. Free surface elevation contours of Test Case III

(Contours are in cm)

The model was applied to compute the velocity and water depth in the junction region using the computational grid of 60x30 shown in Fig 8. Two different values for Manning's roughness coefficient n, 0.013 and 0.016, were imposed upstream and downstream respectively. The larger value at the downstream is due to the irregularity of the bed shown in Fig. 10. Three computations, Test Cases III-1 to III-3, with different β values were performed as detailed in Table 2. It was well observed that larger β caused an increase in the depth. The increase of upstream depth from III-2 to III-3 was found to be 2%. This type of experience is reported and discussed also in Vreugdenhil and Wijbenga (1982). The results of Test Case III-1 with low value of β, $\beta = 0.2$ ($\varepsilon = 3$ cm^2/s) for upstream flat beds and a larger value β, $\beta = 0.5$ ($\varepsilon = 8$ cm^2/s) for the downstream (including the confluence region) are used to compare predictions with observations. The predicted velocity vectors in Fig. 11 compare well with the observations except the rather smooth deflection of the flow at the upstream boundary of the scour hole and faster lateral redistribution. The predicted free surface elevation contours in Fig. 12 well exhibit the free surface superelevation over scour hole and at the right bank across the downstream corner. The backwater effect in the upstream flows is also well predicted.

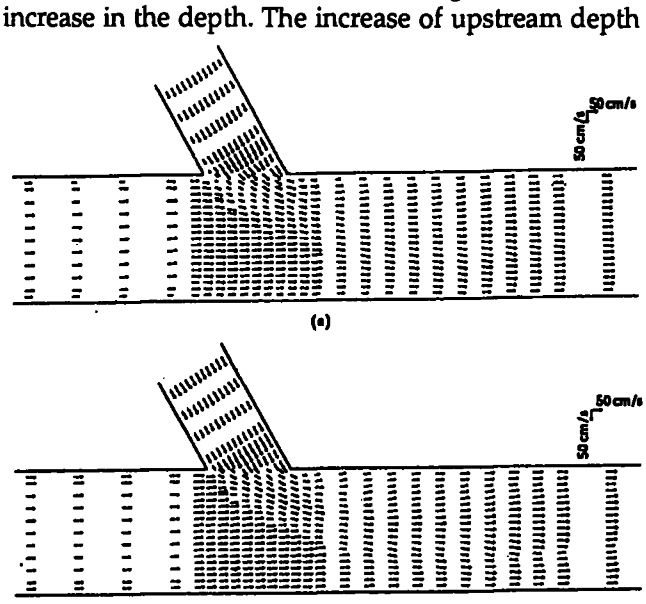

Figure 11. Velocity vectors in Test Case III; a) Computed b) Measured

8. Conclusions

A depth-averaged computational model in orthogonal coordinates suitable for flow computation in shallow water rivers with complex boundary shapes has been presented. The grid generation procedure for obtaining grids at required spacing is based on a quasiconformal mapping method. The flow computational procedure is based on a SIMPLE-like procedure using a new depth correction equation. The model performance including the sensitivity of the effective eddy viscosity was verified by the application of the model to gradually varying flow in a straight channel, in junction flow, with flow recirculation and with a scour hole. It is also shown that the depth-averaged model is capable of providing the flow velocities and water surface elevations satisfactorily in shallow water conditions for design purposes when the Manning roughness and effective viscosity are properly selected. The model was shown to be stable and accurate in the applications for depth-averaged flow computations over irregular bed topography as found in natural rivers. The Paper also includes sufficient details of the grid generation and the flow computation procedures so that an interested engineer can develop, with less effort, his/her own model for obtaining flow patterns of practical problems in river engineering.

References

ASCE 1989 ASCE Task Committee on Turbulence models in Hydraulic Computations, Turbulence modeling of surface water flow and transport. J. Hydr. Engrg. ASCE, 114(9), pp970-1064.

Baburatsi et al.1996 Baburatsi, M., Nassiri M. and Chu V.H., Computation of shallow recirculating flow dominated by friction. J. of Hydraulic Engrg., ASCE, 122(7), pp367-372.

Best 1988 Best, J. L., Sediment transport and bed morphology at river channel confluences. J. Sedimentalogy, 110(11), pp487-498.

Cunge et al. 1980 Cunge, J.A., Holly Jr. F. M. and Verwey A., Practical Aspects of Computational Hydraulics, Pitman Publishing Ltd., London.

Fischer et al. 1979 Fischer, B. F. List E. J. Koh R. C. Y. Imberger J. and Brooks N. H., Mixing in Inland and Coastal Waters. Academic Press ,N. Y.

Kuipers and Vreugdenhil 1973 Kuipers, J. and Vreugdenhil C.B., Calculation two-dimensional horizontal flow. Report S163, Delf Hydraulics Laboratory, Delft, Netherlands.

Lien 1999 Lien, H.C., Hsieh, J.C and Yeh, K.C., Bend flow simulation using 2D depth-averaged model. J. of Hydraulic Engrg., ASCE, 125(10), pp1097-1107.

Molls and Chaudhry 1995 Molls, T. and Chaudhry, W.H., Depth-averaged open-channel flow model. J. of Hydraulic Engrg., ASCE, 121(6), pp453-465.

Patankar 1980 Patankar, S., Numerical Heat Transfer and Fluid Flow, Hemisphere Publications, McGraw Hill Book Co., NY.

Patankar and Spalding 1972 Patankar, S. and Spalding, D., A calculation procedure for heat, mass and momentum transfer in three-dimensional parabolic flows. Int. J. of Heat and Mass Transfer, 15, pp787-1806.

Roahe 1972 Roahe, P.J., Computational fluid Mechanics, Hermosa Publishers, Albuquerque, New Mexico.

Sokolonikoff 1964 Sokolonikoff, I.S. Tensor analysis, John Willy Inc. Publishers, N.Y.

Thompson and Warsi 1982 Thompson, J.F. and Warsi, Z.V.A., Boundary-fitted coordinate systems for numerical solution of partial-differential equations - A review. J. of Computational Physics, 47,pp1-108.

Versteeg and Malalasekera 1995 Versteeg, H.K. and Malalasekera, W., Introduction to computational fluid dynamics : the finite volume method, Wiley Publishers, NY.

Vreugdenhil 1994 Vreugdenhil, C. B., Numerical Methods for Shallow Water Flow, Kluwer Publishers. The Netherlands.

Vreugdenhil and Wijbenga 1982 Vreugdenhil, C. B. and Wijbenga, J. H. A., Computation of flow patterns in rivers. J. Hydr. Div. ASCE, 108(11), pp1296-1310.

Wenka et al. 1993 Wenka, T., Rodi, W. and Nestman, F., Depth-averaged calculation of flow in river reaches with flood control and sediment regulation structures. Proc. 25th Congress of IAHR, Tokyo, A(1), pp41-48.

Weerakoon et al. 1990 Weerakoon, S. B., Tamai, N. and Kawahara, Y., Bed topography, bed shear stress distribution and velocity field in a confluence, Proc. of Hydr. Engrg., JSCE, 1990, 34, pp307-312.

Weerakoon et al. 1991 Weerakoon, S. B., Tamai, N. and Kawahara, Y., A depth correction equation for depth-averaged flow computations in natural rivers. Proc. of Int. Symp. on Environmental Hydraulics, Hong Kong, Vol.2, Balkema Publishers, pp993-998.

Wijbenga 1985 Wijbenga, J. H. A., Determinations of flow patterns in rivers with curvilinear coordinates. Proc. 21st IAHR Congress, Melbourne, 2, pp132-138.

Ye, J. and Mcorquodale1997 Ye, J. And Mcorquodale J.A., Depth-averaged hydrodynamic model in curvilinear collocated grid. J. of Hydraulic Engrg., ASCE, 123(5), pp380-388.

Zhou 1995 Zhou, J G., Velocity-depth coupling in shallow-water flows. J. of Hydraulic Engrg., ASCE, 121(10), pp717-724.